Research Square

Preprints are preliminary reports that have not undergone peer review.
They should not be considered conclusive, used to inform clinical practice,
or referenced by the media as validated information.

Quantification of Choroidal Blood Flow and Structure in High Myopia

Anqi Lei
Xiaogan Hospital, Wuhan University of Science and Technology
Rui Li
Xiaogan Hospital, Wuhan University of Science and Technology
Weiqun Hu
Xiaogan Hospital, Wuhan University of Science and Technology
Zexu Wang
Xiaogan Hospital, Wuhan University of Science and Technology
Chunmei Zou
Xiaogan Hospital, Wuhan University of Science and Technology
Danna Zhang
2419910230@qq.com

Xiaogan Hospital, Wuhan University of Science and Technology

Research Article

Keywords: Choroidal blood flow, Choroidal stroma, High myopia, SS-OCTA, Choroidal capillary density (CCD), Choroidal vessel volume per unit area (CVV/a), Choroidal stroma volume per unit area (CSV/a), Choroidal stroma index (CSI)

Posted Date: July 14th, 2026

DOI: https://doi.org/10.21203/rs.3.rs-9837900/v1

License: This work is licensed under a Creative Commons Attribution 4.0 International License.
Read Full License

Additional Declarations: No competing interests reported.

Abstract

Background

The aim of this study was to use ultra-widefield swept-source optical coherence tomography angiography (SS-OCTA) to investigate the relationship between changes in choroidal structure and blood flow density and the progression of myopia.

Methods

This cross-sectional study included 120 myopic participants aged 18 to 45 years. Based on spherical equivalent (SE), they were grouped as follows: emmetropia and low myopia (− 3.00 D < SE ≤ + 0.75 D), moderate myopia (− 6.00 D < SE ≤ − 3.00 D), and high myopia (SE ≤ − 6.00 D). A 24 mm × 20 mm macular scan was performed using the BM-400K BMizar. The scan area was divided into 9 regions: supra-temporal (ST), temporal (T), infra-temporal (IT), superior (S), central macular area (C), inferior (I), supra-nasal (SN), nasal (N), and infra-nasal (IN), and the following parameters were quantified: choriocapillaris density (CCD), choroidal vascular volume per unit area (CVV/a), choroidal stromal volume per unit area (CSV/a), and choroidal stromal index (CSI).

Results

With increasing myopia severity, CCD and CVV/a decreased significantly in most regions (all $P < 0.05$), while CSI increased compensatorily ($P < 0.05$). Temporal(T) CCD exhibited an inverted U-shaped relationship with axial/corneal radius ratio (AL/CR ratio, AR) ($b_2 = -22.77$, $P < 0.001$, $R^2 = 0.856$), with the inflection point located at an AL/CR ratio of 3.05; CCD increased compensatorily before the inflection point, and decreased significantly after the inflection point. A significant negative correlation was observed between CVV/a and CSI ($r = -0.592$, $P < 0.001$).

Conclusions

Choriocapillaris alterations in highly myopic eyes are neither uniform nor synchronous, showing marked spatiotemporal heterogeneity. The posterior pole showed an early compensatory increase in density, which later gave way to a diffuse decrease. The temporal region decompensated even earlier, suggesting region-specific differences in hypoxia and vascular remodeling. The choroid in highly myopic patients showed atrophic remodeling: CSV/a decreased markedly, while CSI increased.

Introduction

Myopia has become an increasingly serious and widely recognised global public health issue. Currently, the global prevalence of myopia exceeds 28.3%, with the prevalence of high myopia standing at 4.0%. It

is projected that by 2050, the prevalence of myopia will reach 49.8%, whilst that of high myopia will reach 9.8% [1, 2]. The progression of myopia is accompanied by changes in the blood circulation and structural characteristics of the fundus, whilst patients with high myopia often exhibit metabolic abnormalities in the retina and choroid, which significantly affect the blood perfusion of these structures. Furthermore, the mechanical elongation of the axial length of the eye can lead to a reduction in the thickness of the choroid and the retinal pigment epithelium, ultimately resulting in a series of degenerative ocular conditions in patients with high myopia.

Although there have been numerous previous studies focusing on retinal and choroidal blood flow perfusion and thickness in patients with high myopia (HM), most have concentrated on changes in retinal blood flow and thickness, as well as changes in choroidal capillary bed blood flow and choroidal thickness [3, 4], and the majority of these studies have employed an imaging field of 12×12 mm. with very few studies evaluating whether compensatory changes in the choroidal capillary density (CCD) occur in the central and mid-peripheral macula as myopia progresses within a 20×24 mm field of view, or investigating the correlation between total choroidal stroma volume per unit area and the choroidal stroma index, as well as its association with the axial length-to-diameter ratio. Several studies have compared the choroidal imaging capabilities of SS-OCT and spectral-domain OCT (SD-OCT); SS-OCT has been shown to identify the choroidoscleral junction in normal eyes more accurately than SD-OCT (regardless of whether the EDI method is used)[5, 6]. Most previous OCT systems have primarily scanned the macular region [7, 8, 9, 10, 11, 12], with limited ability to detect lesions in the peripheral retina or choroid; consequently, wide-field OCT scanning systems have emerged[13, 14, 15], providing a useful tool for investigating changes in the peripheral choroidal region. The development of SS-OCTA technology facilitates a deeper exploration of choroidal vascular characteristics during the progression of myopia. Accordingly, this study employed super-wide-field swept-source optical coherence tomography angiography (SS-OCTA) with a scanning range of 24 mm × 20 mm to conduct a quantitative comparative analysis of choroidal vascular changes in eyes with high myopia and control eyes. The aim is to further elucidate the mechanisms of choroidal perfusion in high myopia and to provide a theoretical basis for the prevention and control of high myopia, as well as the management of associated pathological changes in the fundus.

Methods

Study participants

A cross-sectional study design was adopted, enrolling 120 eyes from participants who attended Xiaogan Central Hospital between February 2025 and September 2025. Of these, 54 eyes from 54 participants served as the control group, whilst 66 eyes from 66 participants with high myopia formed the high myopia group. For participants in the control group whose both eyes met the inclusion criteria, one eye was randomly selected for inclusion; For participants with high myopia, if both eyes met the inclusion criteria, the eye with the longer axial length was included. Age-matched participants aged 18–50 years

will be divided into three groups based on equivalent spherical equivalent (SE): the emmetropia and low myopia group (-3.00D < SE ≤ + 0.75D), the moderate myopia group (-6.00D < SE ≤ -3.00D) and the high myopia group (SE ≤ -6.00D) [16]. Inclusion criteria for the control group: (1) Age ≥ 18 years; (2) Best-corrected visual acuity (BCVA) ≥ 0.8; (3) -6.0 D < SE ≤ + 0.75 D; (4) Intraocular pressure (IOP) 10–21 mmHg (1 mmHg = 0.133 kPa). Inclusion criteria for the high myopia group: (1) Age ≥ 18 years; (2) SE ≤ −6.0 D or AL ≥ 26.5 mm; (3) intraocular pressure (IOP) of 10–21 mmHg. Exclusion criteria: (1) History of systemic diseases such as hypertension or diabetes; (2) History of vitreous surgery or intravitreal injections; (3) History of fundus diseases such as diabetic retinopathy or retinal detachment; (4) Inability to obtain high-quality fundus images due to poor fixation or severe opacity of the refractive media.

Ophthalmologic examination.

Best-corrected visual acuity was assessed in all participants using a standard logarithmic visual acuity chart. Intraocular pressure was measured using a non-contact tonometer (2X-20, Nidek, Japan). Computerised refraction was performed using a computerised keratometer (KP-800, Topcon, Japan) to determine best-corrected visual acuity and refractive status; an anterior segment examination was performed using a slit-lamp microscope (SLIE, Topcon, Japan), and axial length was measured using an IOLMaster (IOL Master 500, Carl Zeiss Meditec AG, Germany).

Image acquisition protocol.

All subjects were examined using a 400 kHz SS-OCTA device manufactured by Tupai (Beijing) Medical Technology Co., Ltd., with a scan area of 24 mm × 20 mm centred on the fovea, employing a scan mode of 1536 (horizontal) × 1280 (vertical) B-scan grids. The device's built-in artificial intelligence algorithm automatically identifies the Bruch's membrane and the choroidal-scleral interface. The choroidal large vessel layer is defined as the region between 29 μm sub-Bruch's and the choroidal-scleral interface, with the machine's AI technology automatically segmenting the vascular lumen from the stroma. In the en-face view, the scan area is divided into nine equal sections, with the central 8.0 mm × 6.7 mm region serving as the central zone containing the macula. The device's accompanying software is used to automatically measure the choroidal stroma index (CSI), defined as the percentage of choroidal stroma area relative to the total choroidal area; choroidal stromal volume per unit area (CSV/a), which is the volume of the choroidal stroma (non-vascular portion) per unit area; and choriocapillaris flow density (CCD), which is the percentage of the choriocapillaris blood flow signal area relative to the area of the selected region.

Data analysis.

Statistical analyses were performed using SPSS 27.0 (IBM, USA) statistical software. The Kolmogorov–Smirnov test was used to assess the normality of the distribution of continuous variables, which are expressed as mean ± standard deviation. Comparisons between the three groups were performed using the Kruskal–Wallis H test (as the data did not follow a normal distribution), with post-hoc pairwise comparisons adjusted using the Bonferroni correction. Spearman's correlation test was used for

correlation analysis. Non-linear relationships were examined using a quadratic regression model. A p-value of < 0.05 was considered statistically significant.

Results

General Information and ocular characteristics

There were no statistically significant differences in age or gender composition among the three groups ($P > 0.05$); the axial length ratio and equivalent spherical power in the high myopia group were significantly higher than those in the low and moderate myopia groups ($P < 0.05$) (Table 1).

Table 1 Comparison of demographic of subjects between three groups

Character-stics	EaLM	MM	HM	P
Number(eyes)	30	26	65	
Age(y)	31	33	34	0.056
Gender(M/F)	7/22	7/18	27/39	0.2173
AR	3.10 ± 0.09	3.22 ± 0.08	3.44 ± 0.14	<0.01
SE(D)	184.48 ± 83.5	448 ± 85.97	848.67 ± 242.25	<0.01

Regional CCD analysis of choroid

Comparison of CCD across different regions in each group Among the nine regions, significant differences in CCD were observed between the three groups in the nasocentral, superior, temporocentral, nasal, temporal and inferotemporal regions ($P < 0.05$); no statistically significant differences were found in the remaining three regions. (Table 2, Fig. 1)

Table 2
Comparison of CCD across nine regions among patients with different myopia severities

CCD	EaLM(n = 28)	MM(n = 26)	HM(n = 66)	*P*
SN	48.69 ± 2.54	44.24 ± 7.53	44.08 ± 7.66	0.013
S	48.03 ± 1.59	48.36 ± 1.11	46.93 ± 3.46	0.021
ST	47.83 ± 3.78	45.36 ± 4.75	41.45 ± 9.62	0.004
N	46.59 ± 1.74	44.16 ± 3.63	44.45 ± 3.7	0.01
C	46.59 ± 1.52	46.44 ± 1.64	46.14 ± 2.1	0.764
T	45.93 ± 3.37	44.4 ± 3.74	42.44 ± 5.88	0.005
IN	43.03 ± 7.02	40.88 ± 7.0	40.45 ± 7.93	0.209
I	47.24 ± 2.73	47.08 ± 1.87	45.68 ± 5.2	0.163
IT	40.93 ± 6.48	35.32 ± 8.78	35.27 ± 8.89	0.007

Regional CSV/a analysis of choroid

In all nine regions, with the exception of the supra-nasal region, CSV/a values decreased significantly with increasing myopia, and the differences between the three groups were statistically significant ($P < 0.05$). The differences were particularly pronounced in the nasolateral and infra-temporal regions ($P < 0.01$) (Table 3, Fig. 2).

Table 3
Comparison of CSV/a across nine regions among patients with different myopia severities

CSV/a	EaLM(n = 28)	MM(n = 26)	HM(n = 66)	*P*
SN	107.03 ± 26.43	111.12 ± 31.36	95.05 ± 28.45	0.066
S	116.52 ± 38.42	103.84 ± 39.53	91.36 ± 26.71	0.02
ST	109.76 ± 22.34	101.36 ± 20.40	95.24 ± 25.82	0.026
N	99.34 ± 24.86	99.64 ± 28.08	80.92 ± 25.57	< 0.001
C	125.66 ± 44.49	103.4 ± 39.23	89.62 ± 34.36	0.002
T	118.24 ± 36.16	113.68 ± 30.38	96.74 ± 27.59	0.008
IN	71.45 ± 21.03	67.76 ± 15.53	59.89 ± 14.37	0.01
I	82.55 ± 28.58	68.32 ± 22.09	63.36 ± 22.76	0.011
IT	93.07 ± 28.42	91.68 ± 21.86	76.64 ± 20.78	< 0.001

Regional CSI analysis of choroid

In eight regions other than the superior region, there were statistically significant differences in CSI between the three groups ($P < 0.05$). Contrary to the trends observed for VD and CSV/a, CSI values increased with increasing myopia, with the highest CSI observed in the high myopia group (Table 4, Fig. 3).

Table 4
Comparison of CSI across nine regions among patients with different myopia severities

CSI	EaLM(n = 28)	MM(n = 26)	HM(n = 66)	*P*
SN	58.55 ± 14.02	61.08 ± 5.57	60.3 ± 5.97	<0.001
S	60.03 ± 18.82	55.76 ± 2.07	56.82 ± 3.39	0.230
ST	57.48 ± 8.85	56 ± 11.25	61.42 ± 7.08	0.004
N	60.41 ± 17.14	60.2 ± 4.18	61.06 ± 5.3	0.007
C	61.72 ± 15.76	57.12 ± 2.85	59.26 ± 3.23	0.004
T	61.93 ± 9.39	62.72 ± 4.35	63.82 ± 5.65	0.032
IN	61.07 ± 8.30	63.56 ± 5.97	66.15 ± 6.55	< 0.001
I	57 ± 8.49	56.08 ± 2.58	57.71 ± 4.3	0.131
IT	61.03 ± 6.19	64.28 ± 6.57	65.06 ± 6.6	0.010

Inverted U-shaped relationship between CCD and axial ratio

A quadratic regression model was established with the centred axial ratio as the independent variable and the temporal CCD as the dependent variable. The results showed that temporal CCD exhibited a significant inverted U-shaped quadratic relationship with the axial ratio (quadratic term coefficient $b_2 = -22.77$, linear term coefficient $b_1 = -11.85$, both $P < 0.001$, $R^2 = 0.856$). The calculated inflection point was at an axial ratio of 3.05. When the axial ratio was < 3.05, temporal CCD exhibited a compensatory upward trend; once this threshold was exceeded, CCD decreased significantly as the axial ratio increased (Fig. 4). The results indicate a significant inverted U-shaped relationship between temporal VD and the axial ratio, suggesting that compensatory increases in vascular density occur during the early stages of axial length growth, followed by a decompensatory decline once the threshold is exceeded.

The correlation between CSV/a and CSI

Spearman's correlation analysis revealed a significant negative correlation between CSV/a and CSI ($r = -0.592$, $P < 0.001$), indicating that as CSV/a increases, CSI decreases, reflecting an inverse compensatory relationship. (Figs. 5 and 6)

Discussion

The choroid [17] is a highly vascularised tissue situated between the sclera and Bruch's membrane. Its primary function is to supply oxygen and nutrients to the outer layers of the retina via blood flow [18]; other functions include light absorption, thermoregulation, and the regulation of intraocular pressure through the modulation of choroidal blood flow [19]. Research has shown that the choroid can also adjust the position of the retina through changes in its thickness, as well as release growth factors involved in regulating angiogenesis, scleral remodelling and ocular growth [20, 21, 22, 23]. Abnormalities in choroidal blood volume or impaired blood flow can lead to photoreceptor dysfunction and death [24].

It is currently believed that changes in choroidal vascular structure and blood flow may play a significant role in the development of myopic retinal pathology [11, 25, 26]. Previous studies suggest that the choroid is involved not only in the pathogenesis of various choroidoretinal diseases but also in the regulation of ocular growth and the development of myopia. It is worth noting that a recent study by Zhang et al. found that reduced choroidal blood flow perfusion is a major contributing factor to the progression of myopia in humans [27], and there is a growing consensus that the choroid plays a significant role in ocular growth and the development of abnormal refractive states such as myopia [28]. Therefore, elucidating changes in choroidal structure and vascular characteristics during the progression of myopia is crucial for in-depth research into its pathological mechanisms, as well as for the prevention and treatment of high myopia. This study utilised ultra-wide-field SS-OCTA to perform quantitative analyses of vascular and matrix indices in multiple choroidal subregions of eyes with varying degrees of myopia. The results demonstrated that as myopia progressed from low to high severity, CCD and CSV/a progressively decreased in most regions, whilst CSI compensatorily increased, presenting a typical microcirculatory change pattern characterised by 'structural reduction and functional compensation'.

Previous studies have shown that choroidal capillary blood flow density is reduced in individuals with high myopia, primarily occurring in the 3–6 mm peripheral zone [29], with no significant differences observed in mild to moderate myopia. This suggests that choroidal thinning is primarily caused by the loss of the Haller and Sattler layers, rather than capillary loss, a change observed exclusively in high myopia[30, 31]. However, the present study found that, with the exception of the central, inferior nasal and inferior regions, the choroidal capillary density (CCD) in all other areas decreased significantly with increasing myopia, with the most pronounced decline observed in the temporal and inferior temporal regions. This indicates that the sparseness of choroidal capillaries in high myopia is not uniform, but is more pronounced in the temporal macula and the mid-periphery. Cao et al. [32] proposed that in children with mild to moderate myopia, not only is perfusion of medium and large choroidal vessels reduced, but capillary perfusion is also diminished. Furthermore, in our non-linear analysis, we found that the relationship between CCD and the axial ratio is not a simple linear negative correlation, but rather an inverted U-shaped relationship that first increases and then decreases, with the inflection point occurring at an axial ratio of approximately 3.05. In the early stages of axial elongation, local capillaries can still temporarily increase blood flow density through compensatory dilation to maintain retinal perfusion;

however, once the axial ratio exceeds a critical threshold, the capillary network becomes compressed and sparse, perfusion loses its compensatory capacity, and CCD decreases significantly. This dynamic process suggests that the axial ratio may serve as a potential turning-point indicator for the transition from compensation to decompensation in myopic choroidal ischaemia, and thus holds clinical predictive value.

CSV/a represents the volume of choroidal stroma per unit area and constitutes the absolute volume of the choroidal stroma. We found that, with the exception of the superior nasal region, CSV/a decreased significantly across all regions as the degree of myopia increased, with the most pronounced decreases observed in the nasal and inferior temporal regions; this distribution pattern largely overlaps with the regions where CCD is reduced. The decrease in CSV/a implies that, as myopia progresses, the absolute volume of the choroidal stroma progressively decreases, and the overall structural organisation of the choroid undergoes atrophy. However, the choroidal stroma index (CSI) conversely increases, with the most pronounced rise observed in peripheral regions such as the inferior nasal and inferior temporal areas. An increase in CSI represents a rise in the proportion of stromal components within the total choroidal area. This seemingly contradictory phenomenon actually carries significant pathophysiological implications: when the overall thickness of the choroid decreases and its total volume diminishes, if the rate of atrophy of the vascular lumen exceeds the rate of collapse of the stromal components, the relative proportion of stroma within the remaining choroidal tissue is passively increased. The significant negative correlation between CSV/a and CSI ($r = -0.592$) precisely confirms this asymmetric remodelling pattern—the concurrent occurrence of a reduction in the absolute volume of the stroma (decrease in CSV/a) and an increase in its relative proportion (increase in CSI) indicates that, during the reduction of total choroidal volume, the loss of vascular components is more severe than that of stromal components. From an anatomical perspective, the choroidal capillary layer lacks a complete muscular wall structure and is more susceptible to collapse, occlusion and atrophy under the mechanical traction caused by axial elongation; whilst the large vessel layer, although possessing a thicker smooth muscle wall, is also unable to fully resist persistent passive dilation, ultimately manifesting as luminal narrowing and reduced blood flow. This characteristic of differential remodelling—marked by ‘overall volume atrophy, more pronounced vascular loss, and relative matrix accumulation’—reflects the dynamic pathophysiological process by which the microcirculation of the fundus in high myopia transitions from a compensatory to a decompensatory state, and can serve as a sensitive imaging indicator for assessing myopic choroidal atrophy and vascular loss.

This study has certain limitations: firstly, the sample size is relatively small, and it is a single-centre cross-sectional study that fails to track the dynamic evolution of individual microcirculation longitudinally; secondly, we only selected the central and mid-peripheral regions of the macula, excluding the most peripheral areas from the analysis. Furthermore, metabolic and oxygenation indices were not measured concurrently, and inferences regarding the mechanisms of compensation and decompensation require further validation. Future research should involve large-scale, multicentre prospective studies, combined with functional examinations, to further explore the key turning points and optimal intervention timing in choroidal remodelling associated with high myopia.

In summary, changes in choroidal capillaries in patients with high myopia are not uniform or synchronous, but rather exhibit marked spatiotemporal heterogeneity: In the early stages, the posterior pole first exhibits compensatory increases in density, which gradually evolve into diffuse decreases as the condition progresses, whereas the paracentral and peripheral regions enter a state of decompensation at an earlier stage. Choroidal vascular remodelling also exhibits layer-specific characteristics, specifically manifested by the simultaneous presence of decreased CCD, decreased CSV/a, and a relative increase in CSI, presenting a trend of mutually independent changes. These findings provide new imaging evidence for understanding myopic choroidal ischaemia and vascular remodelling. Furthermore, the quantitative indices obtained through the non-invasive SS-OCTA technique are expected to serve as a useful reference for the early warning and follow-up monitoring of retinal pathologies in high myopia.

Declarations

Ethics approval and consent to participate

All subjects gave their informed consent for inclusion before they participated in the study. This study was conducted in strict adherence to the ethical principles outlined in the Declaration of Helsinki, and it received approval from the Ethics Committee of Xiaogan Hospital Affiliated to Wuhan University of Science and Technology. (Project identification code: XGSZXYYLL-EC-2025062508. Date of approval: 2025-6-30). Informed consent was obtained from all subjects involved in the study.

Consent for publication

Not applicable

Conflict of interest

The authors declare that they have no competing interests.

Funding

This study was funded by the Natural Science Foundation of Xiaogan

Province, China (grant numbers: XGKJ202410047).

Author Contribution

AL concepted, drafted, and revised the manuscript. RL drafted the manuscript. AL,ZW, and CZ collected and analysed data. WH and DZ provided comments and revised the manuscript. All authors read and approved the final version of the manuscript.

Acknowledgements

Not applicable.

Data Availability

The raw data supporting this study cannot be shared publicly due to restrictions imposed by the hospital ethics committee concerning patient privacy. However, the data will be made available from the corresponding author upon reasonable request, subject to ethical clearance and the signing of a data use agreement.

References

1. Holden BA, Fricke TR, Wilson DA, Jong M, Naidoo KS, Sankaridurg P, et al. Global Prevalence of Myopia and High Myopia and Temporal Trends from 2000 through 2050. Ophthalmology. 2016;123(5):1036–42. 10.1016/j.ophtha.2016.01.006. . Epub 2016 Feb 11.
2. Baird PN, Saw SM, Lanca C, et al. Myopia Nat Rev Dis Primers. 2020;6(1):99. 10.1038/s41572-020-00231-4.
3. AZEMIN M Z C, DAUD N M, AB HAMID F, et al. Influence of refractive condition on retinal vasculature complexity in younger subjects[J]. ScientificWorldJournal. 2014;2014. 10.1155/2014/783525 . Epub 2014 Oct 13.
4. SHIMADA N, OHNO-MATSUI K, HARINO S, et al. Reduction of retinal blood flow in high myopia[J]. *Graefe's Archive For Clinical and Experimental Ophthalmology = Albrecht V on Graefes Archiv Fur*. Klinische Und Experimentelle Ophthalmologie. 2004;242(4):284–8. 10.1007/s00417-003-0836-0 . Epub 2004 Jan 14.
5. CopeteS F-MI et al. MonteroJA,. Direct comparison of spectral-domain and swept-source OCT in the measurement of choroidal thickness in normal eyes[J]. *Br J Ophthalmol*, 2014, 98(3): 334–338. 10.1136/bjophthalmol-2013-303904
6. AdhiM LJJ. Choroidal analysis in healthy eyes using swept-source optical coherence tomography compared to spectral domain optical coherence tomography[J]. Am J Ophthalmol. 2014;157(6):1272–e12811. 10.1016/j.ajo.2014.02.034.
7. LiuL ZC. Three-dimensional choroidal vascularity index in high myopia using swept-source optical coherence tomography[J]. Curr Eye Res. 2022;47(3):484–92. 10.1080/02713683.2021.2006236.
8. WangY CS. Vascular changes of the choroid and their correlations with visual acuity in pathological myopia[J]. Invest Ophthalmol Vis Sci. 2022;63(12):20. 10.1167/iovs.63.12.20.
9. WuH ZG. Assessment of choroidal vascularity and choriocapillaris blood perfusion in anisomyopic adults by SS-OCT/OCTA[J/OL]. Invest Ophthalmol Vis Sci. 2021;62(1):8. 10.1167/iovs.62.1.8.

10. ZhengF CJ. Quantitative OCT angiography of the retinal microvasculature and choriocapillaris in highly myopic eyes with myopic macular degeneration[J]. Br J Ophthalmol. 2022;106(5):681–8. 10.1136/bjophthalmol-2020-317632.
11. MilaniP MG. Vessel density, retinal thickness, and choriocapillaris vascular flow in myopic eyes on OCT angiography[J]. Graefes Arch Clin Exp Ophthalmol. 2018;256(8):1419–27. 10.1007/s00417-018-4012-y.
12. LuoH SJ. Compartmental analysis of three-dimensional choroidal vascularity and thickness of myopic eyes in young adults using SS-OCTA[J/OL]. Front Physiol. 2022;13:916323. 10.3389/fphys.2022.916323.
13. McNabbRP GDS. Wide field of view swept-source optical coherence tomography for peripheral retinal disease[J]. Br J Ophthalmol. 2016;100(10):1377–82. 10.1136/bjophthalmol-2015-307480.
14. LimHB KK. A comparison of choroidal thicknesses between pachychoroid and normochoroid eyes acquired from wide-field swept-source OCT[J/OL]. Acta Ophthalmol. 2021;99(1):e117–23. 10.1111/aos.14522.
15. Hoseini-YazdiH VSJ. Wide-field choroidal thickness in myopes and emmetropes[J/OL]. Sci Rep. 2019;9(1):3474. 10.1038/s41598-019-39653-w.
16. Chinese Optometric Association of Chinese Medical Association, Optometry Committee of Chinese Ophthalmologist Association of Chinese Medical Doctor Association. Expert consensus on prevention and control of high myopia (2023). Chin J Optometry Ophthalmol Visual Sci. 2023;25(06):401–7. 10.3760/cma.j.cn115909-20230509-00147.
17. Read SA, Fuss JA, Vincent SJ, Collins MJ, Alonso-Caneiro D. (2019) Choroidal Changes in Human Myopia: Insights from Optical Coherence Tomography Imaging. *Clin Exp Optom.* 2019;102(3):270–285. 10.1111/cxo.12862
18. Gonzales AL, Paikai A, Maeng DC. (2025). Interplay of Retinal and Choroidal Vasculatures in Ocular Health and Disease. *Adv Exp Med Biol.* 2025;1468:459–463. 10.1007/978-3-031-76550-6_75
19. NicklaDL WJ. The multifunctional choroid[J]. Prog Retin Eye Res. 2010;29(2):144–68. 10.1016/j.preteyeres.2009.12.002.
20. Liang R, Yang R, Ai B, Tao L, Wang L, Zhou X. (2024). Structural changes in the retina and choroid in patients with different degrees of myopia. *Sci Rep.* 2024;14(1):31033. 10.1038/s41598-024-82142-y
21. Ostrin LA, Harb E, Nickla DL, Read SA, Alonso-Caneiro D, Schroedl F, Kaser-Eichberger A, Zhou X, Wildsoet CF. (2023). IMI—The Dynamic Choroid: New Insights, Challenges, and Potential Significance for Human Myopia. *Invest Ophthalmol Vis Sci.* 2023;64(6):4. 10.1167/iovs.64.6.4
22. Liu Y, Wang L, Xu Y, Pang Z, Mu G. (2021). The influence of the choroid on the onset and development of myopia: from perspectives of choroidal thickness and blood flow. *Acta Ophthalmol.* 2021;99(7):730–738. 10.1111/aos.14773
23. MathisU, ZiemssenF SF. Effects of a human VEGF antibody (Bevacizumab) on deprivation myopia and choroidal thickness in the chicken[J]. Exp Eye Res. 2014;127:161–9. 10.1016/j.exer.2014.07.022.

24. An S, Yu H, Islam MM, Zhang X, Zhan Y, Olivieri JJ, Ambati J, Yao J, Gelfand BD. (2023). Effects of donor-specific microvascular anatomy on hemodynamic perfusion in human choriocapillaris. *Sci Rep*. 2023;13(1):22666. 10.1038/s41598-023-48631-2
25. Si Y, Pang K, Song Y, Zhang X, Yang H, Cui Y. (2024). Observation of structural and vascular features of retina and choroid in myopia using ultra-widefield SS-OCTA. *BMC Ophthalmol.* 2024;24(1):208. 10.1186/s12886-024-03473-y
26. Sun L, Xue M, Tang Y, Zhao C, Li S, Ding W-Q et al. (2024). Association of choroidal thickness and blood flow features with asymmetric axial lengths in children with unilateral myopic anisometropia. *BMC Ophthalmol.* 2024;24(1):329. 10.1186/s12886-024-03616-1
27. Zhang S, Zhang G, Zhou X, Xu R, Wang S, Guan Z, et al. Changes in Choroidal Thickness and Choroidal Blood Per-fusion in Guinea Pig Myopia. Invest Ophthalmol Vis Sci. 2019;60(8):3074–83. 10.1167/iovs.18-26397.
28. Liu Y, Wang L, Xu Y, Pang Z, Mu G. (2021). The influence of the choroid on the onset and development of myopia: from perspectives of choroidal thickness and blood flow. *Acta Ophthalmol.* 2021;99(7):730–738. 10.1111/aos.14773
29. Cheng W, Song Y, Gao X, Lin F, Li F, Wang P, et al. Axial length and choriocapillaris flow deficits in nonpathological high myopia. Am J Ophthalmol. 2022;244:68–78. 10.1016/j.ajo.2022.08.005.
30. Si Y, Pang K, Song Y, Zhang X, Yang H, Cui Y. Observation of structural and vascular features of retina and choroid in myopia using ultra-widefield SS-OCTA. BMC Ophthalmol. 2024;24(1):208–208. 10.1186/s12886-024-03473-y.
31. Liang R, Yang R, Ai B, Tao L, Wang L, Zhou X. Structural changes in the retina and choroid in patients with different degrees of myopia. Sci Rep. 2024;14(1):31033–31033. 10.1038/s41598-024-82142-y.
32. Cao Y, Gu X, Zhang Y, et al. Assessment of the effects of myopic and hyperopic anisometropia on choroidal vascular structure in children using SS-OCTA[J]. Ophthalmic Physiol Opt. 2024;44(3):525–36. 10.1111/opo.13300.

Figures

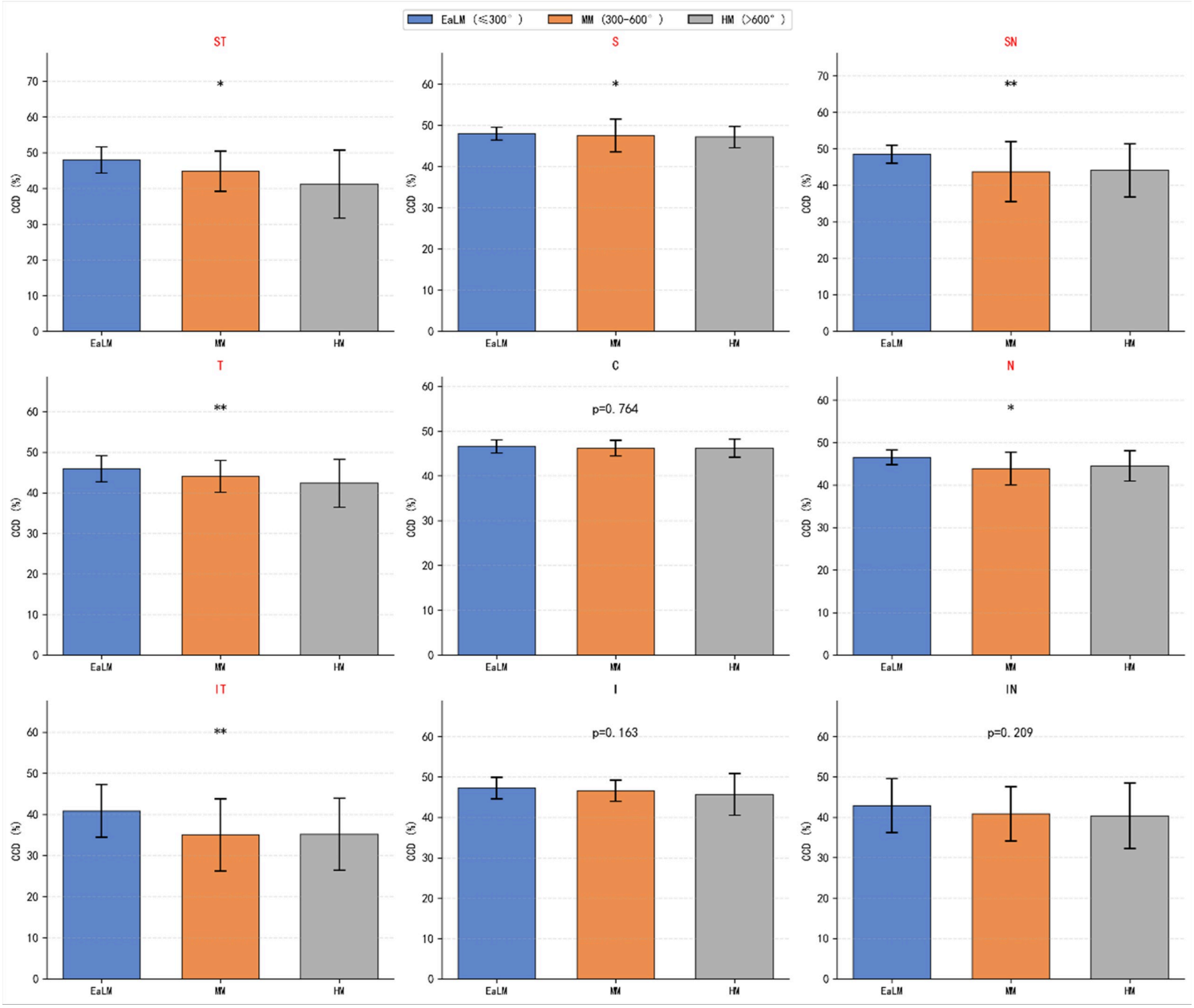


Figure 1

A histogram of comparison of choriocapillaris density across nine regions among three groups with different degrees of myopia. EaLM, emmetropia and low myopia (≤300 D); MM, moderate myopia (300–600 D); HM, high myopia (>600 D). ST, supra-temporal; S, superior; SN, supra-nasal; T, temporal; C, central; N, nasal; IT, infra-temporal; I, inferior; IN, infra-nasal. Data are presented as mean ± SD. Significance markers: *P<0.05, **P<0.01, ***P<0.001.

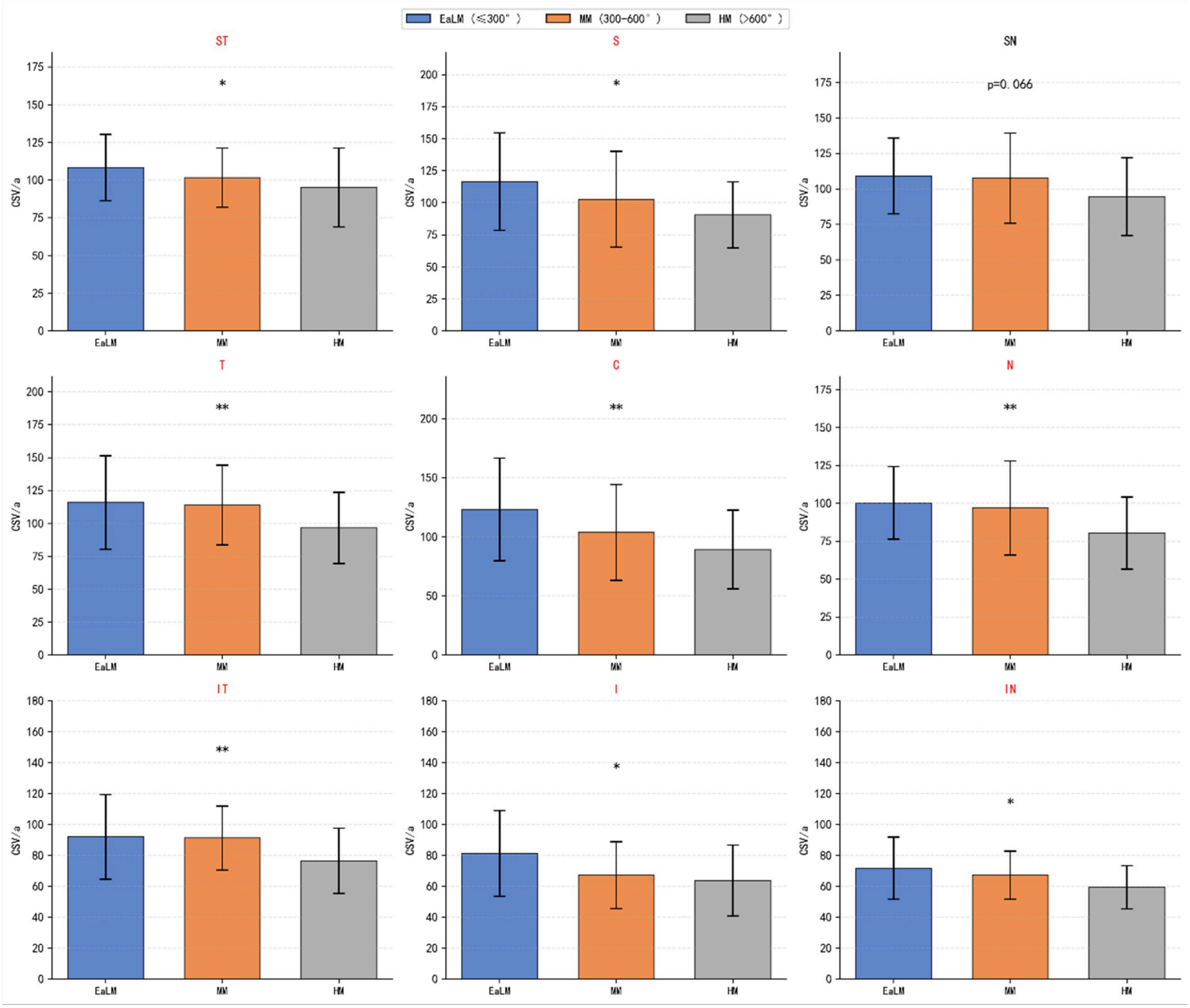


Figure 2

A histogram of comparison of choroidal vascular volume/area ratio (CSV/a) across nine regions among three groups with different degrees of myopia. EaLM, emmetropia and low myopia (≤300 D); MM, moderate myopia (300–600 D); HM, high myopia (>600 D). ST, supra-temporal; S, superior; SN, supra-nasal; T, temporal; C, central; N, nasal; IT, infra-temporal; I, inferior; IN, infra-nasal. Data are presented as mean ± SD.

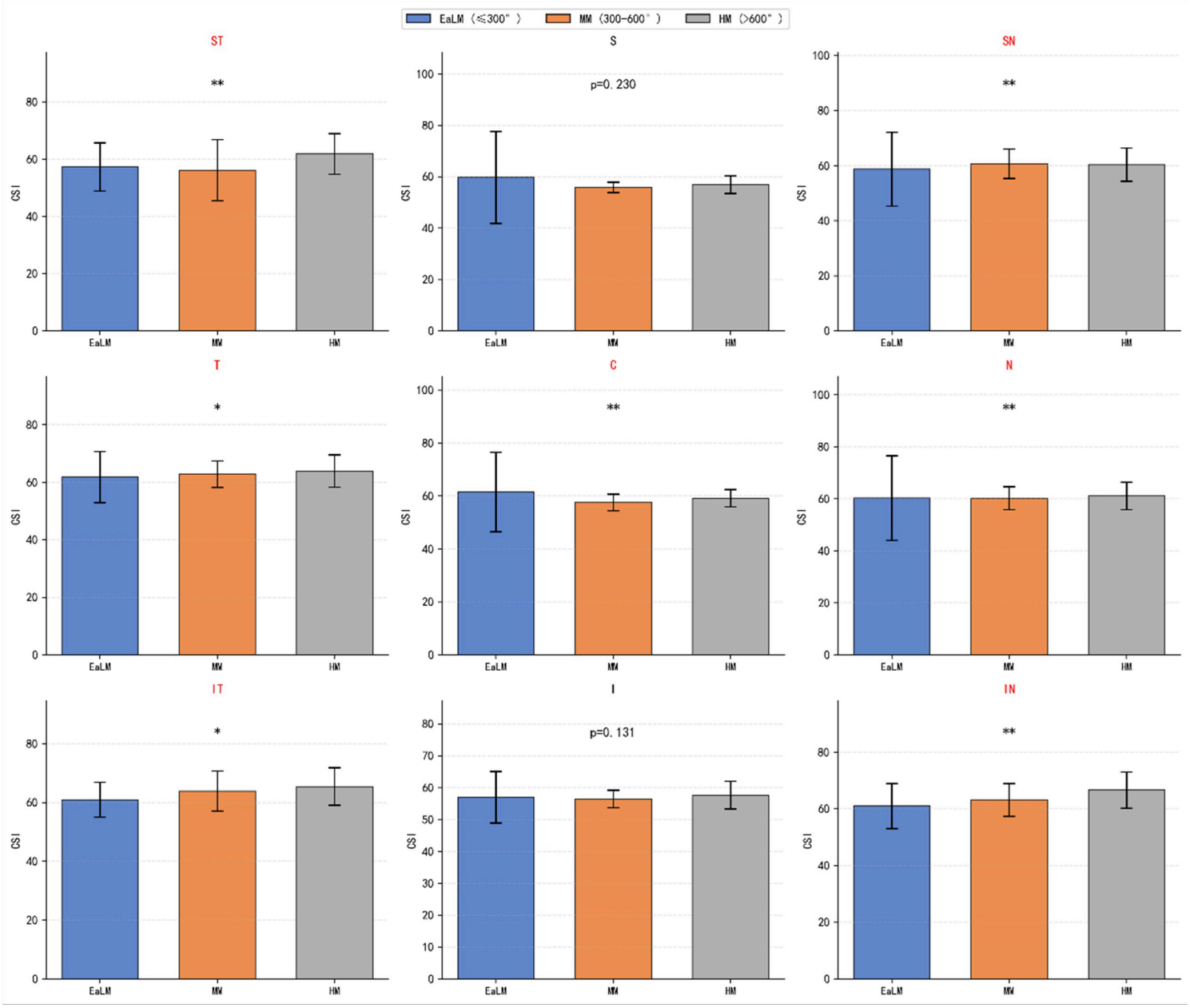


Figure 3

A histogram of comparison of Choroidal Stromal Index across nine regions among three groups with different degrees of myopia. EaLM, emmetropia and low myopia (≤300 D); MM, moderate myopia (300–600 D); HM, high myopia (>600 D). ST, supra-temporal; S, superior; SN, supra-nasal; T, temporal; C, central; N, nasal; IT, infra-temporal; I, inferior; IN, infra-nasal. Data are presented as mean ± SD.

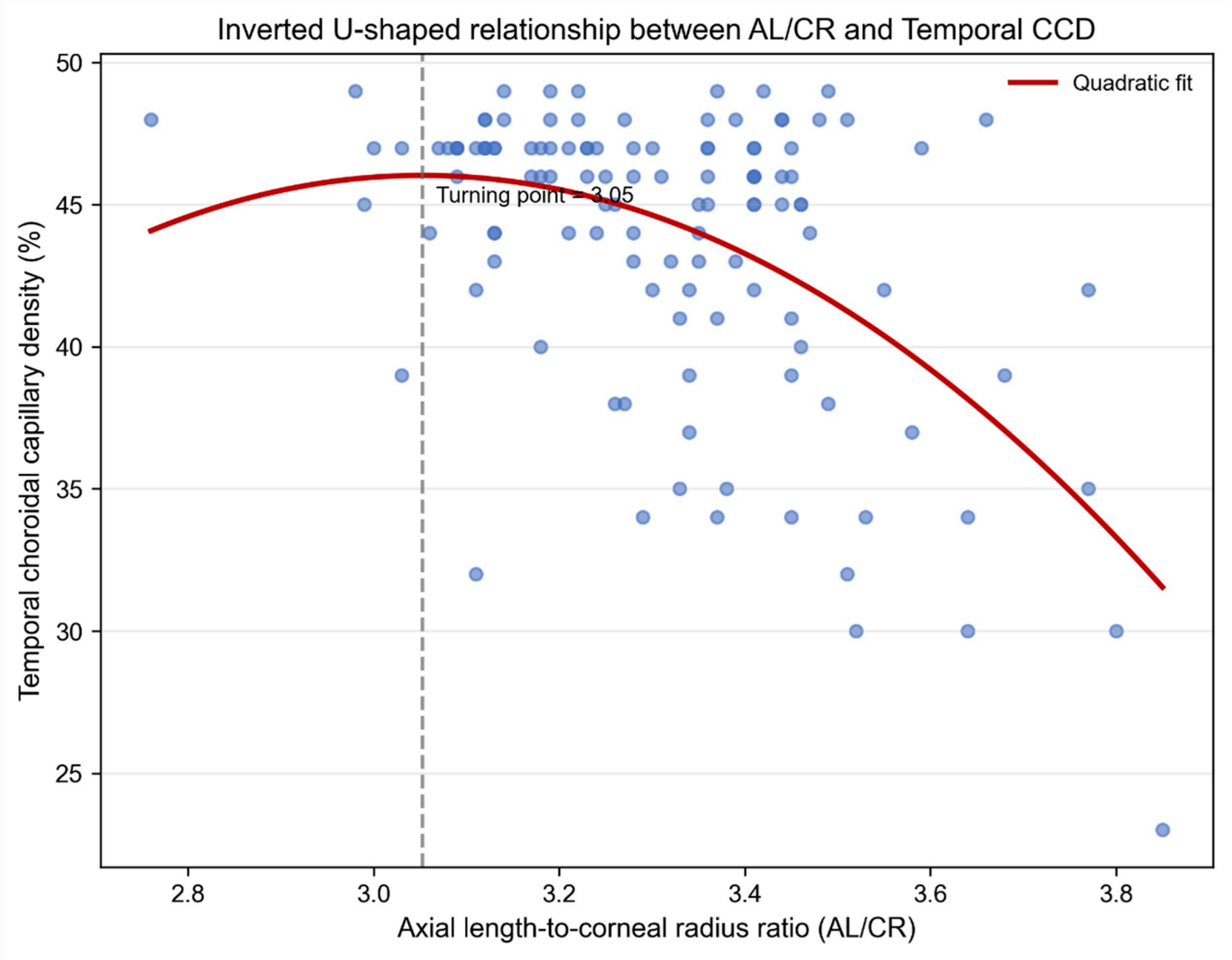


Figure 4

Inverted U-shaped relationship between temporal choroidal capillary density (CCD temporal) and axial length-to-corneal radius ratio (AL/CR). Quadratic regression was performed after centering AL/CR. The quadratic term was significantly negative (coefficient = −22.77, $P < 0.001$), indicating an inverted U-shape. The turning point (peak) was calculated as AL/CR = 3.05 (vertical gray dashed line). Red solid line: fitted quadratic curve. Scatter points represent individual eyes. This result suggests that CCD temporal initially increases with AL/CR up to the turning point and then decreases.

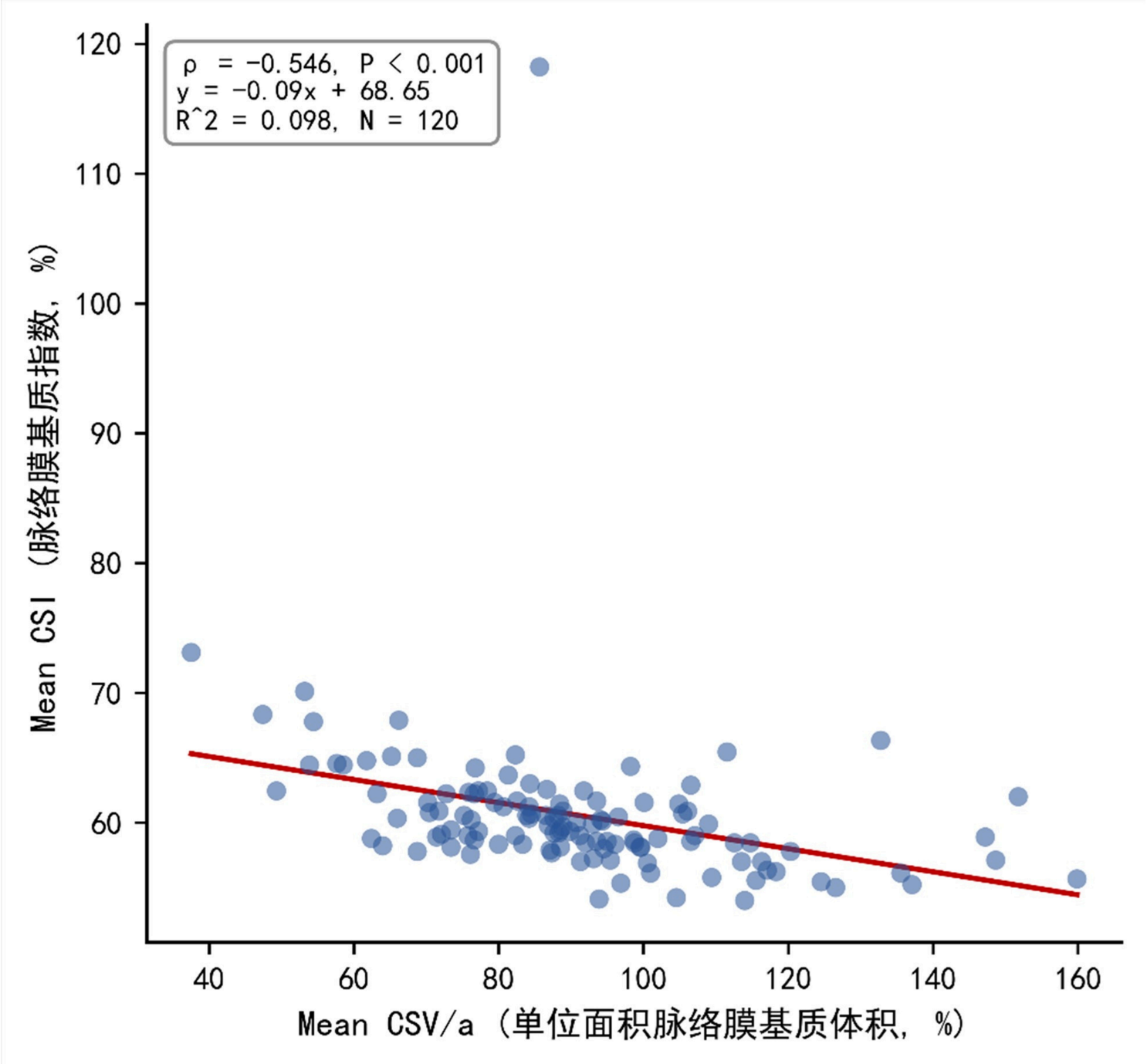


Figure 5

Scatter plot showing the correlation between choroidal stromal volume per area (CSV/a) and choroidal stromal index (CSI). Both CSV/a and CSI were averaged across nine subfields. The red solid line represents the linear regression fit. ρ, Spearman correlation coefficient; R^2, coefficient of determination. *N* = 120.

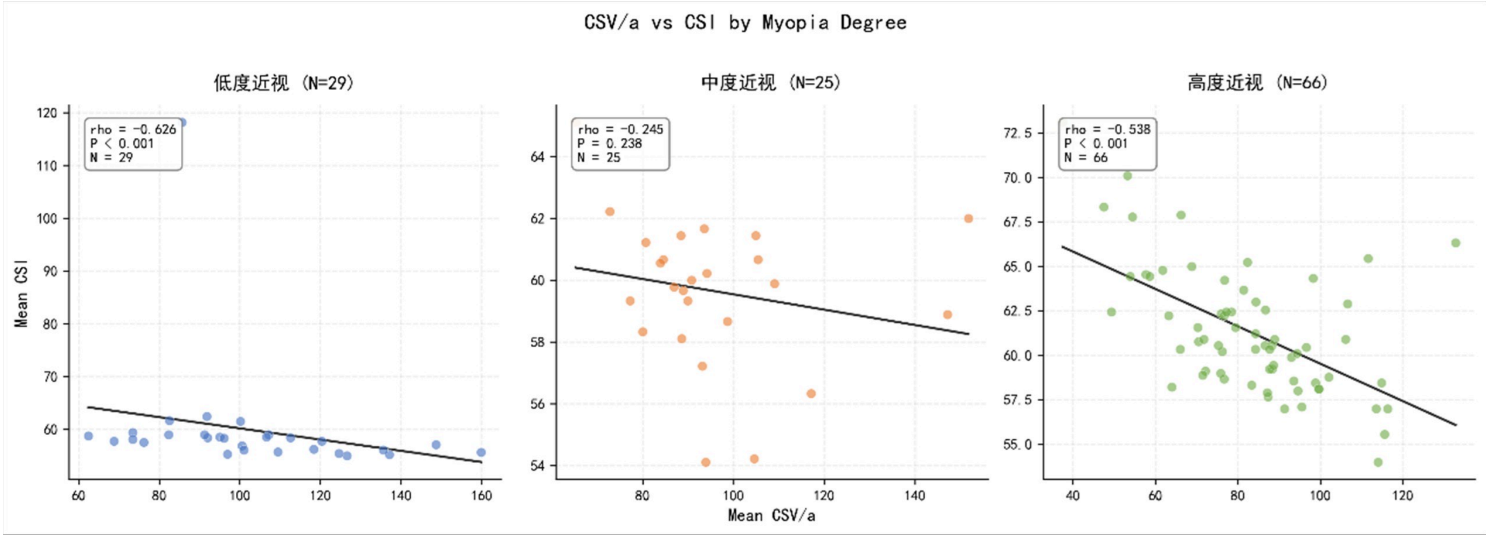


Figure 6

Scatter plots of the correlation between CSV/a and CSI in subgroups stratified by myopia severity. (A) Low myopia group; (B) Moderate myopia group; (C) High myopia group. The solid line in each panel shows the linear fit; ρ indicates the Spearman correlation coefficient, and N refers to the sample size of each group.